atmosphere

MDPI

Article

Correlations between $PM_{2.5}$ and Ozone over China and Associated Underlying Reasons

Jia Zhu [1,2], Lei Chen [1,3], Hong Liao [1,*] and Ruijun Dang [4]

1 Jiangsu Key Laboratory of Atmospheric Environment Monitoring and Pollution Control, Jiangsu Collaborative Innovation Center of Atmospheric Environment and Equipment Technology, School of Environmental Science and Engineering, Nanjing University of Information Science & Technology, Nanjing 210044, China
2 Research Institute of Climatic and Environmental Governance, Nanjing University of Information Science & Technology, Nanjing 210044, China
3 Key Laboratory of Meteorological Disaster, Ministry of Education (KLME), Joint International Research Laboratory of Climate and Environment Change (ILCEC), Collaborative Innovation Center on Forecast and Evaluation of Meteorological Disasters (CIC-FEMD), Nanjing University of Information Science & Technology, Nanjing 210044, China
4 University of Chinese Academy of Sciences, Beijing 100049, China
* Correspondence: hongliao@nuist.edu.cn

Received: 4 June 2019; Accepted: 24 June 2019; Published: 27 June 2019

Abstract: We investigated the spatial-temporal characteristics of the correlations between observed $PM_{2.5}$ and O_3 over China at a national-scale level, and examined the underlying reasons for the varying $PM_{2.5}$–O_3 correlations by using a chemical transport model. The $PM_{2.5}$ concentrations were positively correlated with O_3 concentrations for most regions and seasons over China, while negative correlations were mainly observed in northern China during winter. The strongest positive $PM_{2.5}$–O_3 correlations with correlation coefficients (r) larger than +0.7 existed in southern China during July, and the strongest negative correlations ($r < -0.5$) were observed in northern China during January. It was a very interesting phenomenon that the positive $PM_{2.5}$–O_3 correlations prevailed for high air temperature samples, while the negative correlations were generally found in cold environments. Together, the effective inhibitory effect of $PM_{2.5}$ on O_3 generation by reducing photolysis rates and the strong titration effect of freshly emitted NO with O_3 contributed to the strongest negative $PM_{2.5}$–O_3 correlations in northern China during January (i.e., in cold environments). The strongest positive correlations in southern China during July (i.e., at high temperature), however, were mainly attributed to the promoting effect of high O_3 concentration and active photochemical activity on secondary particle formation.

Keywords: $PM_{2.5}$; ozone; correlation; temperature

1. Introduction

Fine particulate matter with a diameter of 2.5 μm or less ($PM_{2.5}$) is an important pollutant in the atmosphere. Epidemiological studies have revealed a robust correlation between $PM_{2.5}$ levels and the morbidity of cardiovascular and respiratory diseases [1,2]. In addition, $PM_{2.5}$ has strong extinction abilities, and therefore, reduces atmospheric visibility and affects traffic safety [3,4]. Tropospheric ozone (O_3), as another air pollutant, has adverse effects on human health, ecosystems, and crop growth [5–8].

At present, haze and ozone pollution are the most serious atmospheric environmental problems in China [9–16]. However, the formation reasons for the complex air pollution characterized by $PM_{2.5}$ and O_3 are very complex. Although the two important pollutants have different formation mechanisms, the interactions between them lead to close connections and relations. The complex physical and

chemical properties of $PM_{2.5}$ may affect the generation and loss of O_3 [12,17], while O_3 may influence atmospheric oxidizing capacity, and therefore, affect the formation of secondary $PM_{2.5}$ [18,19]. The interactions between $PM_{2.5}$ and O_3 lead to certain correlations of observed concentrations; however, the observed correlations may vary in different seasons and different regions [20–25]. Revealing the rule for $PM_{2.5}$–O_3 correlations over China, as well as investigating the underlying reasons/mechanisms for the $PM_{2.5}$–O_3 correlations, is the scientific basis and an essential requirement for the coordinated control of complex air pollution.

The $PM_{2.5}$ may reduce O_3 concentrations by altering the photolysis rate. The main components of $PM_{2.5}$, such as sulfate, nitrate, black carbon, and organic carbon, can scatter and absorb solar radiation directly, and can also alter the optical properties and life cycle of clouds by becoming cloud condensation nuclei, which in turn, decrease the intensity of incident ultraviolet radiation and finally reduce the photolysis rate and O_3 generation [26–31]. Li et al. [29] investigated the impact of particulates on O_3 via changing photolysis frequencies and reported that the boundary layer O_3 below 1 km was reduced by 5.4% over central Eastern China in June 2006. A high O_3 concentration indicates a strong atmospheric photochemical reactivity, which can promote the formation of secondary particles [19,32–35]. By analyzing concentrations of $PM_{2.5}$, its compositions and gas pollutants measured at a rural site (Dian Shan Lake supersite) in the eastern Yangtze River Delta from 23 July to 11 August 2013, Wang et al. [19] found that strong correlations existed between solar radiation and the production rate of sulfate by gas-phase oxidation, between day-time nitrate and nitrogen dioxide (NO_2) and O_3, and between secondary organic aerosol (SOA) and O_x (O_3+NO_2), which indicated that the formation of secondary particles (sulfate, nitrate, and SOA) was promoted by photochemical oxidation.

Certain correlations between $PM_{2.5}$ and O_3 were reported in several cities of China, and the observed $PM_{2.5}$–O_3 correlations varied in different seasons and different regions [20–25,36–39]. Xu et al. [36] analyzed observed pollutant concentrations in Beijing and reported that $PM_{2.5}$ concentrations were negatively correlated with O_3 concentrations with a correlation coefficient (r) of −0.51 in February 2003, but no statistically significant correlations were found in August 2003. By analyzing the observed pollutant concentrations provided by Shanghai Environment Monitoring Center, Shi et al. [38] revealed that $PM_{2.5}$ concentrations were positively correlated (r = +0.59) with O_3 concentrations during ozone-rich days in July and August 2013.

Previous studies revealed correlations between surface-layer $PM_{2.5}$ and O_3 concentrations over China. However, these studies mostly focused on the individual city and season, which could not make clear representative sense for comprehensively understanding the $PM_{2.5}$–O_3 correlations over the whole of China. Furthermore, most of these studies only mentioned the relevant phenomenon, while the reasons for the $PM_{2.5}$–O_3 correlations have been poorly understood. Although some studies revealed interactions between $PM_{2.5}$ and O_3, the impacts of $PM_{2.5}$–O_3 interactions on their correlations, especially the importance of different interactions in different regions and seasons, are still unclear and need to be further investigated.

This paper aimed to (1) obtain the spatial-temporal characteristics of the correlations between $PM_{2.5}$ and O_3 at a national-scale level, based on the pollutant concentrations measured at all monitoring sites of China for the whole year 2016, and (2) examine the underlying mechanisms on the varying $PM_{2.5}$–O_3 correlations in different regions and seasons using a chemical transport model (GEOS-Chem). The obtained knowledge is expected to provide a scientific basis for the coordinated control of complex air pollution over China. The methods, including descriptions of in situ measurements, data analysis, and model configuration are presented in Section 2. Section 3 shows the results, including observed $PM_{2.5}$–O_3 correlations, model evaluation, and underlying reasons/mechanisms. The conclusion and discussion are presented in Section 4.

2. Methods

2.1. In Situ Measurements and Data Analysis

The Ministry of Ecological and Environment (MEE), formerly the Ministry of Environmental Protection of the People's Republic of China (MEP), has begun to release to the public the real-time monitoring air quality data of six criteria pollutants including $PM_{2.5}$ and O_3 covering most cities in China since 2013. The observation sites in each city are designed as a mix of urban and background sites, with most of the sites located in urban areas. According to China's Environmental Protection Standards, the β absorption method and the micro oscillating balance method are used to continuously measure $PM_{2.5}$ concentrations ("HJ 653-2013"), while the ultraviolet spectrophotometry method is used to automatically monitor O_3 concentrations ("HJ 654-2013").

The hourly $PM_{2.5}$ and O_3 concentrations can be obtained from the MEE website, from which we downloaded the concentrations at 1497 sites of the whole China for year 2016. For each site, the negative or missing values were removed; those sites with less than 80% valid data were also abandoned. Although the MEE provides hourly $PM_{2.5}$ and O_3 concentrations, the National Ambient Air Quality Standards (NAAQS, GB3095-2012) sets limits on annual or daily mean concentrations for $PM_{2.5}$ and maximum daily 8 h average (MDA8) or hourly mean concentrations for O_3. For consistency, we calculated daily mean $PM_{2.5}$ concentration and daily MDA8 O_3 concentration to conduct correlation analysis. Following the NAAQS, we conducted the validity treatment for data statistics as follows: the daily average $PM_{2.5}$ concentrations were calculated when there were valid data for more than 20 h during that day; the 8 h average O_3 concentrations were calculated when there were valid data for at least 6 h for every 8 h. Pearson correlation coefficients (r) were calculated for correlation analysis.

The meteorological data of surface temperature over China for the year 2016, which will be used in Section 3.1 to examine the temperature dependence of $PM_{2.5}$–O_3 correlations, were extracted from the re-analysis dataset of the ERA-Interim in the European Centre for Medium-Range Weather Forecasts (ECMWF) [40]. These gridded observation records with a horizontal resolution of 0.25° × 0.25° were then bilinearly interpolated to the corresponding air quality monitoring stations, as was done in Wang et al. [41] and Zhong et al. [42].

2.2. Model Configuration

To investigate the reasons for the varying $PM_{2.5}$–O_3 correlations in different regions and seasons, we needed to obtain concentrations of $PM_{2.5}$ components, photolysis rates, etc., at all sites over China for the year 2016, which were almost unavailable from in situ measurements. Therefore, a chemical transport model (GEOS–Chem) was used to reproduce the observed $PM_{2.5}$–O_3 correlations and examine the underlying mechanisms. It was easy to output concentrations of $PM_{2.5}$ components, photolysis rates, and other variables for the chemical transport model.

The simulations of $PM_{2.5}$ and O_3 were carried out with the nested-grid version of the GEOS-Chem model, which included detailed ozone–NO_x–VOC–aerosol chemistry [43], with a horizontal resolution of 0.5° latitude × 0.625° longitude (version 11-01). The nested domain was set over Asia (60°–150° E, 11° S–55° N), and the chemical boundary conditions that were updated every 3 h were provided by the global GEOS-Chem simulation with 2° latitude × 2.5° longitude resolution. The simulation was driven by the assimilated MERRA-2 meteorological data from the Goddard Earth Observing System (GEOS) of the NASA Global Modeling Assimilation Office (GMAO) [44]. Over the Asian domain, MIX 2010 was taken as the baseline anthropogenic inventory [45], and the scaling factors after year 2010 followed Zheng et al. [46]. The biomass burning emissions were taken from the Global Fire Emissions Database (GFED4) [47]. Natural emissions, including NO_x from lighting and soil and VOCs from vegetation, were calculated on the basis of MERRA-2 meteorological parameters. The GEOS-Chem simulation was conducted from 1 January to 31 December of the year 2016 after a 6 month model spin-up.

3. Results

3.1. Observed $PM_{2.5}$–O_3 Correlations

Figure 1 shows the spatial-temporal distributions of correlations between daily $PM_{2.5}$ and MDA8 O_3 concentrations over China. Each panel represents each month for the year 2016. It is too intensive to display all 1497 sites on the map, therefore, we present the correlations for all 360 cities. The $PM_{2.5}$ concentrations were positively correlated with O_3 concentrations for most regions and seasons over China, while the negative correlations mainly existed in northern China during winter. The strongest positive correlations ($r > +0.7$) were observed in southern China during July, and the strongest negative correlations ($r < -0.5$) were observed in northern China during January, with most cities passing the 95% confidence level.

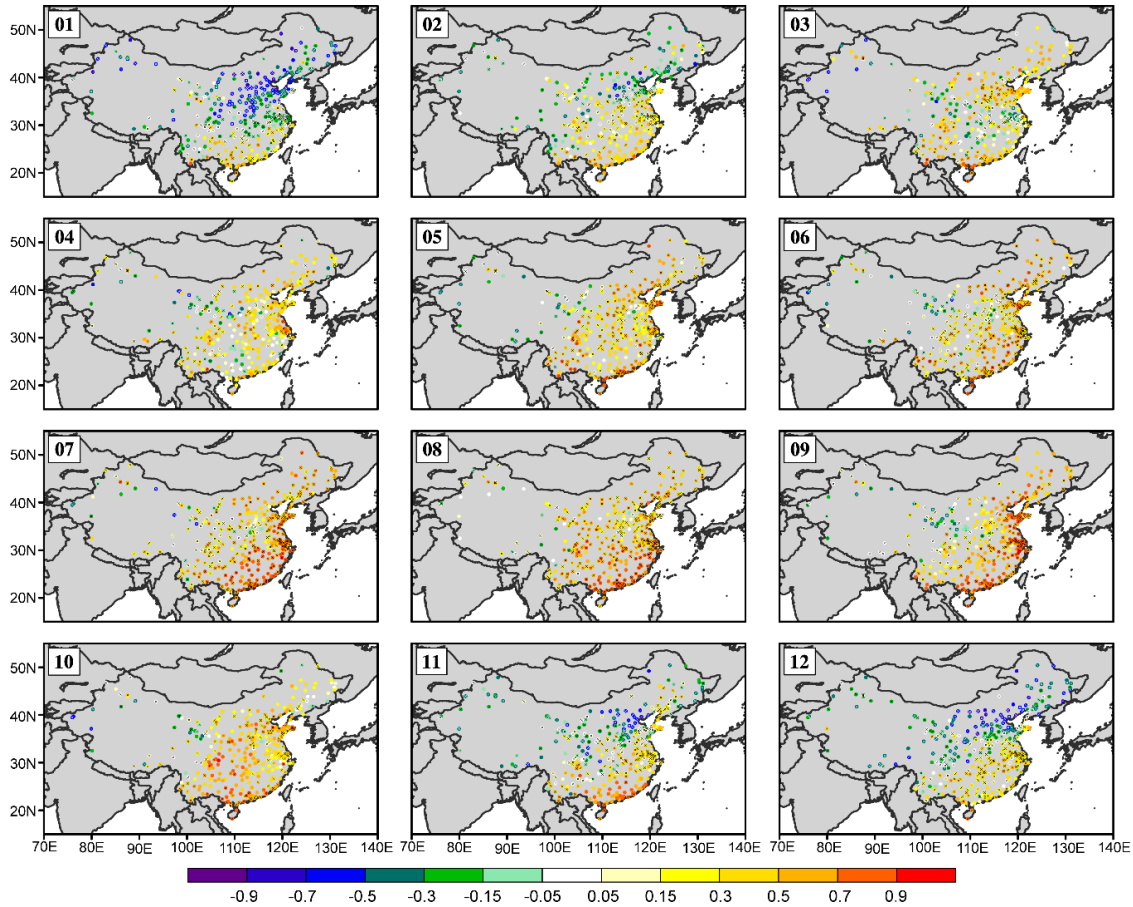

Figure 1. Spatial-temporal distributions of correlations between observed daily $PM_{2.5}$ and maximum daily 8 h average (MDA8) O_3 concentrations over China. Each panel represents each month for the year 2016. The dots with crosses are statistically significant at the 95% level.

Interestingly, the spatial-temporal distributions of $PM_{2.5}$–O_3 correlations highly resembled those of temperature (shown in Figure S1). Both the $PM_{2.5}$–O_3 correlations and temperature reached the maximum in southern China during July and reached the minimum in northern China during January. To further investigate the relations between $PM_{2.5}$–O_3 correlations and temperature, we provide scatter plots of daily $PM_{2.5}$ and MDA8 O_3 concentrations color coded with temperature for all cities of the whole China during 2016 in Figure 2a. Regularly, a positive correlation between $PM_{2.5}$ and O_3 was found for high air temperature samples, while a negative correlation prevailed in cold environments. The phenomenon can be presented more clearly when the data points are separated into northern cities (shown in Figure 2b) and southern cities (shown in Figure 2c). A remarkable positive correlation was

found for high temperature over southern China and a significant negative correlation was observed for low temperature over northern China, which was also well reflected in Figure 1. It was noted that the relations between $PM_{2.5}$–O_3 correlations and other meteorological parameters (e.g., relative humidity) were much weaker (scatter plots for other meteorological parameters were not shown).

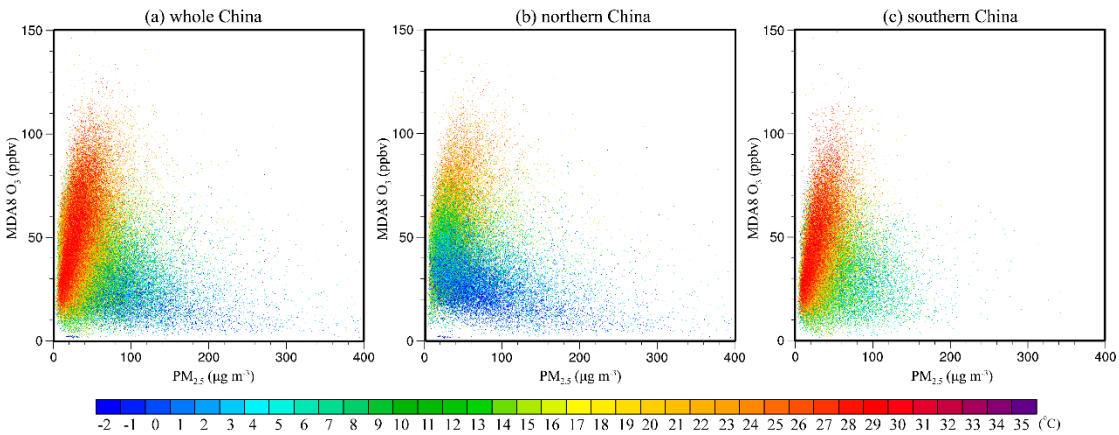

Figure 2. Scatter plots of observed daily $PM_{2.5}$ and MDA8 O_3 concentrations color coded with temperature for all cities of the (**a**) whole China, (**b**) northern China, and (**c**) southern China during the year 2016. Northern (southern) China is defined as the area north (south) of 33° N.

In the following sections, we focus on comparing data points which exhibit the strongest positive $PM_{2.5}$–O_3 correlations and high air temperature (i.e., southern China in July) and those that exhibit the strongest negative $PM_{2.5}$–O_3 correlations and low air temperature (i.e., northern China in January), to investigate the underlying reasons for the varying $PM_{2.5}$–O_3 correlations.

3.2. Model Evaluation

Previous studies have indicated that the GEOS-Chem model captures the distributions of observed $PM_{2.5}$ [13,48,49] and O_3 [11,50–52] over China fairly well. We conducted comparisons with the MEE measurements here to evaluate whether the version of the GEOS-Chem model used in this study can reproduce the observed variations in surface-layer $PM_{2.5}$ and O_3 and their correlations.

The observed and simulated daily $PM_{2.5}$ and MDA8 O_3 concentrations for northern cities in January and southern cities in July are shown in Figures 3 and 4, respectively. Although the model generally underestimated (overestimated) the absolute $PM_{2.5}$ (MDA8 O_3) concentrations, the model successfully captured the temporal variations of $PM_{2.5}$ and MDA8 O_3 concentrations. For northern cities in January, the correlation coefficients between the simulated and observed $PM_{2.5}$ (MDA8 O_3) concentrations ranged from 0.70 to 0.87 (from 0.67 to 0.89); for southern cities in July, the correlation coefficients for $PM_{2.5}$ (MDA8 O_3) were in the range of 0.52 to 0.80 (0.79 to 0.92). For both observed and simulated concentrations, $PM_{2.5}$ presented an overall negative correlation with MDA8 O_3 in northern China during January but exhibited a significant positive correlation with MDA8 O_3 in southern China during July. The observed inverse correlations were reproduced by the GEOS-Chem model fairly well. Therefore, it was feasible to conduct $PM_{2.5}$–O_3 correlation analysis using the GEOS-Chem model.

3.3. Underlying Reasons and Mechanisms

As mentioned in the Introduction, there exist interactions between $PM_{2.5}$ and O_3. However, $PM_{2.5}$ and O_3 may exhibit varying and even inverse correlations in different seasons and different regions, which indicates that the importance of different interactions on the $PM_{2.5}$–O_3 correlations may vary over time across space. The Beijing–Tianjin–Hebei (BTH, 37°–41° N, 114°–118° E) agglomeration, as the representative of northern China, has a low temperature below 0 °C and the strongest negative $PM_{2.5}$–O_3 correlation in January. The Pearl River Delta (PRD, 22°–24° N, 112°–115° E) agglomeration,

as the representative of southern China, has a high temperature above 27 °C and the strongest positive $PM_{2.5}$–O_3 correlation in July. Therefore, in this section, we chose the BTH in January (as the representative of negative $PM_{2.5}$–O_3 correlations and low temperature) and PRD in July (as the representative of positive $PM_{2.5}$–O_3 correlations and high temperature), to compare the importance of different $PM_{2.5}$–O_3 interactions on the correlations for different regions and seasons (i.e., different temperature) and reveal the underlying reasons/mechanisms, based on the GEOS-Chem simulation.

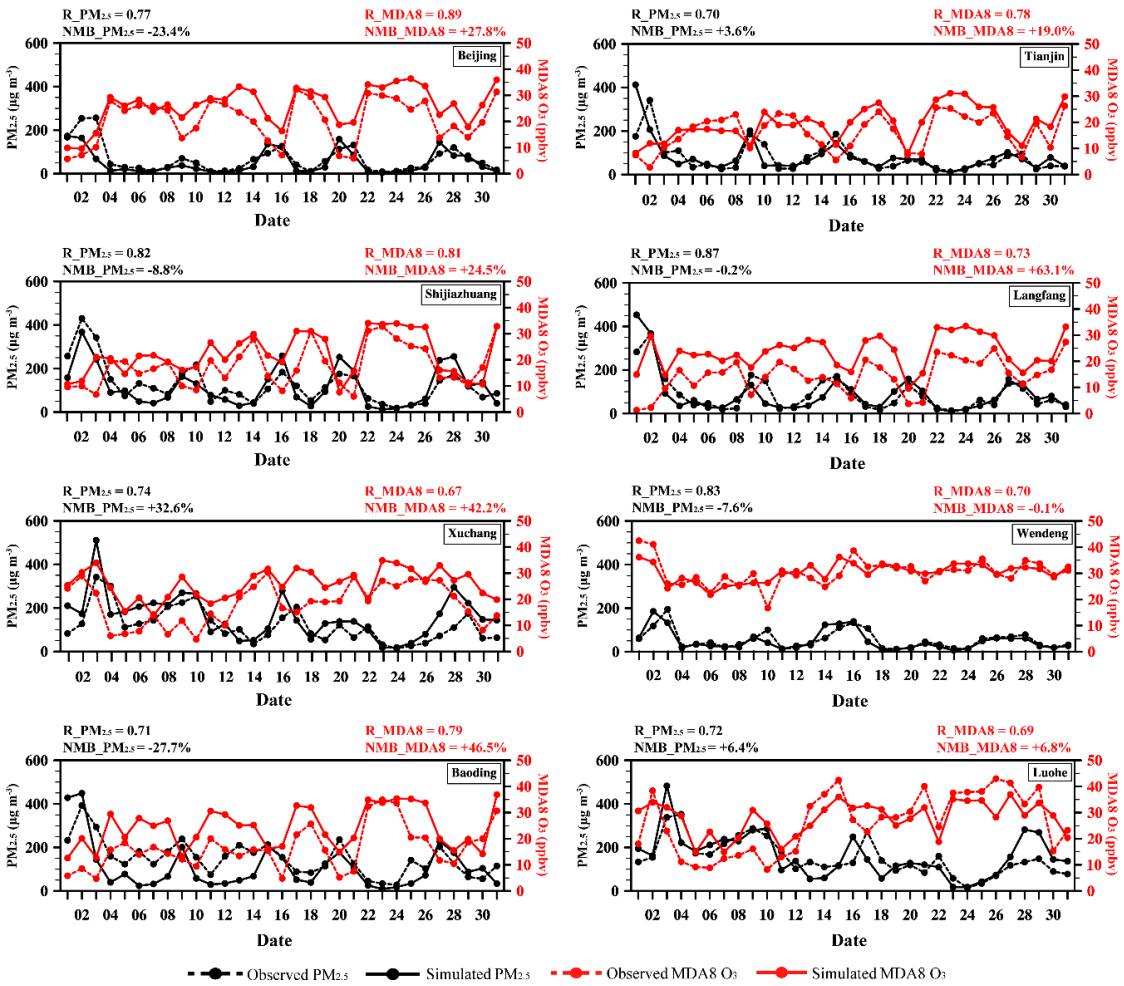

Figure 3. Observed and simulated daily $PM_{2.5}$ and MDA8 O_3 concentrations for northern cities in January. Observed (simulated) concentrations are shown in dashed (solid) lines. The $PM_{2.5}$ (MDA8 O_3) concentrations are shown in black (red) lines. The correlation coefficient (*r*) and normalized mean bias (NMB) between the observations and simulations are shown above each panel.

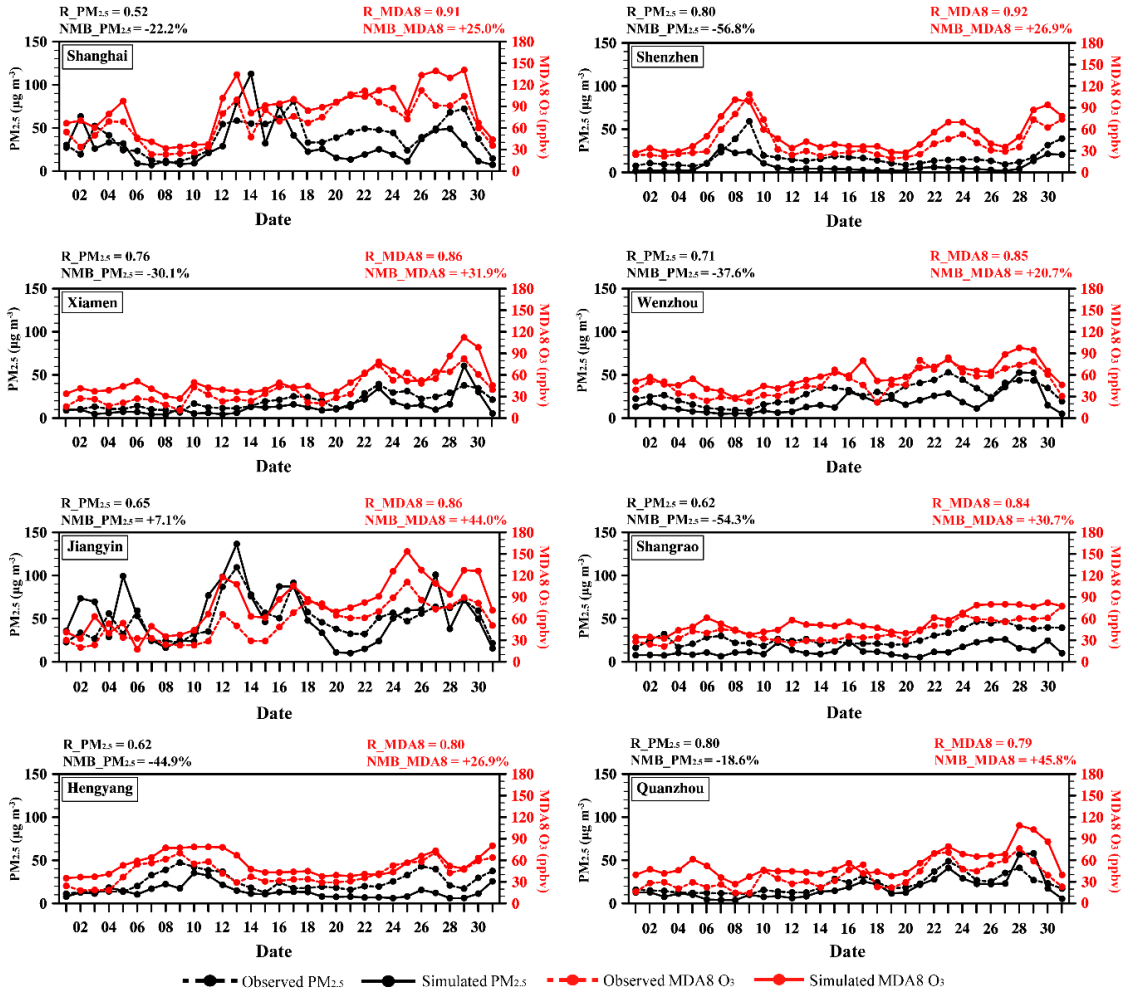

Figure 4. Observed and simulated daily $PM_{2.5}$ and MDA8 O_3 concentrations for southern cities in July. Observed (simulated) concentrations are shown in dashed (solid) lines. The $PM_{2.5}$ (MDA8 O_3) concentrations are shown in black (red) lines. The correlation coefficient (*r*) and normalized mean bias (NMB) between the observations and simulations are shown above each panel.

3.3.1. $PM_{2.5}$ Suppressing O_3 Generation by Reducing Photolysis Rates

Particulates may decrease the actinic flux of incident solar radiation by scattering or absorbing solar radiation directly and altering the optical properties of clouds indirectly, and inhibit the photolysis reactions near the surface by reducing the photolysis rates, which finally reduce the O_3 generation [26–31].

Figure 5 shows the time-series of simulated daily $PM_{2.5}$ concentrations, solar radiation at the ground (RADSWG), photolysis rates ($J(NO_2)$ and $J(O_3)$), and MDA8 O_3 concentrations, for BTH in January and PRD in July. It is remarkable in Figure 5a that the RADSWG was negatively correlated with $PM_{2.5}$ ($r = -0.45$), indicating the strong extinction effects of particulates on solar radiation. The photolysis rates, including $J(NO_2)$ and $J(O_3)$, and MDA8 O_3 concentrations presented significantly positive correlation with RADSWG, which finally resulted in a strongly negative correlation between $PM_{2.5}$ and MDA8 O_3 for BTH in January. Influenced by meteorological conditions, the $PM_{2.5}$ concentrations exhibited spikes and valleys. When the $PM_{2.5}$ concentrations reached the peaks, the RADSWG, photolysis rates, and MDA8 O_3 concentrations reached the lowest levels due to the inhibitory effect of $PM_{2.5}$ on O_3 generation by reducing photolysis rates. By contrast, for PRD in July (Figure 5b), the correlation between RADSWG and $PM_{2.5}$ was much smaller ($r = -0.27$), indicating a weaker extinction effect of particulates on solar radiation and a consequently weaker influence on

photolysis rates and MDA8 O_3 concentrations. For BTH in January, the average $PM_{2.5}$ concentrations were relatively high because of winter heating and low boundary layer height associated with low temperature, which led to a more effective suppressing effect of $PM_{2.5}$ on O_3 generation by reducing photolysis rates for cold environments. A similar phenomenon has also been reported by Tie et al. [26], who pointed out that surface photolysis rates $J(NO_2)$ and $J(O_3)$ in Eastern China were reduced by 10–30% and 20–30% due to the effect of particulates on photolytic radiation in winter, as well as 1–10% and 5–20% in summer, leading to reductions in surface O_3 concentrations by 2–4% in winter and less than 2% in summer. Overall, the negative $PM_{2.5}$–O_3 correlation for cold environment may be partly attributed to the effective inhibitory effect of $PM_{2.5}$ on O_3 generation by reducing photolysis rates at low temperature.

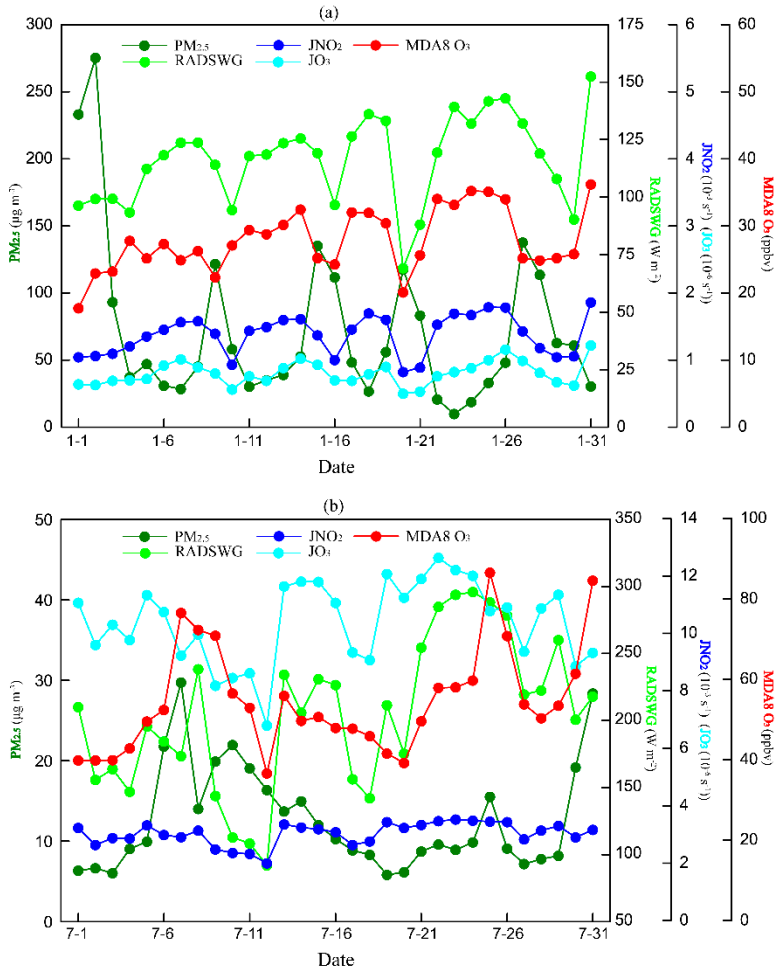

Figure 5. Time-series of simulated daily $PM_{2.5}$ concentrations, solar radiation at the ground (RADSWG), photolysis rates ($J(NO_2)$ and $J(O_3)$), and MDA8 O_3 concentrations for (**a**) Beijing–Tianjin–Hebei (BTH) in January and (**b**) Pearl River Delta (PRD) in July.

3.3.2. NO Suppressing O_3 Production through the NO Titration Effect

It is known that excessive NO is not favorable for O_3 generation. If NO levels are high, O_3 production is suppressed by the "$O_3 + NO \rightarrow NO_2 + O_2$" reaction, usually referred to as NO titration, which is an important O_3 removal process associated with freshly emitted NO [14,53].

The time-series of simulated daily $PM_{2.5}$, BC, NO, and MDA8 O_3 concentrations, for BTH in January and PRD in July, are shown in Figure 6. The NO concentration was calculated to be 8.5 ppbv averaged over BTH in January, six times that for PRD in July. It is conspicuous, in Figure 6a, that the MDA8 O_3 was negatively correlated with NO with a high correlation coefficient of −0.74, indicating a

strong NO titration effect for BTH in January. When the NO concentrations reached the spikes, the MDA8 O_3 concentrations reached the valleys due to the strong NO titration effect. By contrast, the NO titration effect for PRD in July was weaker; the correlation coefficient between MDA8 O_3 and NO was −0.55. Ding et al. [20] and Chen et al. [25] also reported similar finding that the negative correlation mainly existed for low temperature data, suggesting a titration effect of freshly emitted NO with O_3 in cold seasons.

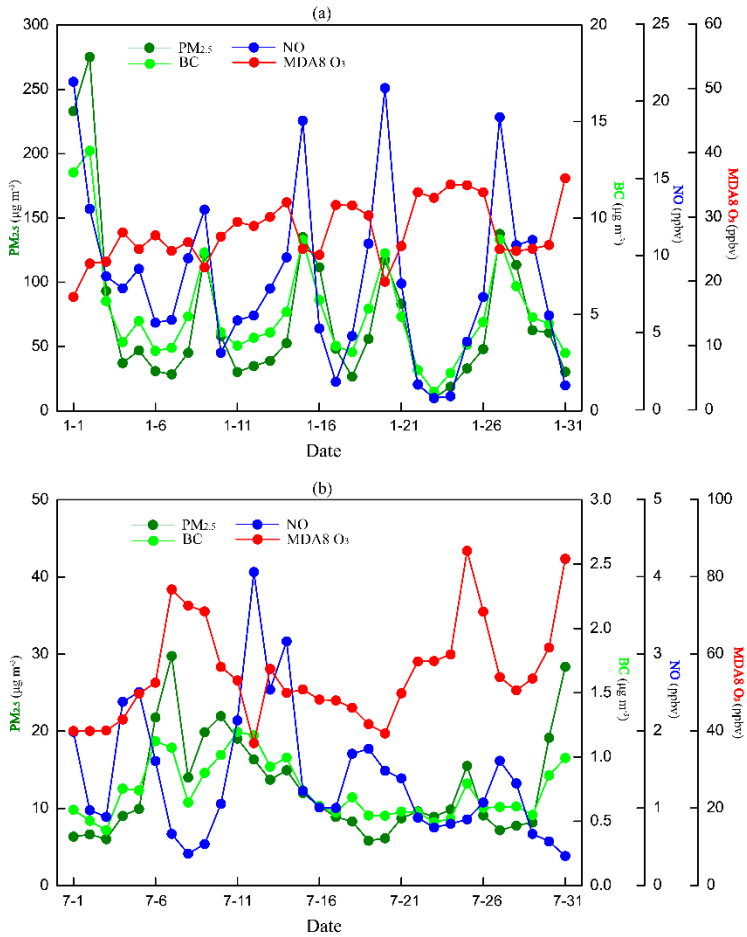

Figure 6. Time-series of simulated daily concentrations for $PM_{2.5}$, black carbon (BC), NO, and MDA8 O_3 for (**a**) BTH in January and (**b**) PRD in July.

For BTH in January, the lower air temperature (generally indicating the feebler solar radiation) resulted in weaker atmospheric oxidation ability, therefore, more NO was freshly emitted. The BC, as a primary particulate, was difficult to generate or clear through chemical reactions. It is noted that NO and BC, as well as $PM_{2.5}$, have similar sources, such as combustion and traffic activities [20,25]. Therefore, the freshly emitted NO presented a significant positive correlation with the primary particulate BC (r = 0.85) and consequently with $PM_{2.5}$ (r = 0.73). In contrast, for PRD in July, more NO was converted to NO_2, and therefore, NO tended to be less correlated with the primary particulate BC (r = 0.39) and consequently with $PM_{2.5}$ (r = −0.13) (Figure 6b).

In conclusion, the significant negative correlation between NO and MDA8 O_3, and the remarkable positive correlation between NO and $PM_{2.5}$, led to the negative correlation between $PM_{2.5}$ and MDA8 O_3 for BTH in January. The negative $PM_{2.5}$–O_3 correlation at low temperature may be partly attributed to the strong titration effect of high NO concentration, which is consistent with primary $PM_{2.5}$ in a cold environment.

3.3.3. High O_3 Concentration and Active Photochemical Activity Promoting Secondary $PM_{2.5}$ Formation

As reported in previous studies, high O_3 concentration generally indicates strong atmospheric photochemical reactivity, which can promote the secondary particulate formation. For example, the photochemical oxidation of SO_2 to H_2SO_4 may be promoted by strong atmospheric photochemical reactions, and the formation of HNO_3 can be strongly enhanced by high O_3 [19,32].

To examine the effects of O_3 and photochemical activity on secondary particulate formation under different temperature conditions, we compared the time-series of simulated daily O_x and MDA8 O_3 concentrations, SOR and NOR, as well as SNA and $PM_{2.5}$ concentrations between BTH in January and PRD in July in Figure 7. The total oxidant O_x ($O_x = O_3 + NO_2$) was used to characterize the atmospheric oxidation capacity, following Wang et al. [14], Jia et al. [22], and Clapp and Jenkin [54]. The sulfur oxidation ratio, SOR = n-SO_4^{2-}/(n-SO_4^{2-} + n-SO_2), was a measure of the conversion degree of sulfur; the nitrogen oxidation ratio, which was defined as NOR = n-NO_3^-/(n-NO_3^- + n-NO_2), was used to quantitatively express the conversion degree of nitrogen [55–58]. The secondary inorganic particulate was defined as SNA = SO_4^{2-} + NO_3^- + NH_4^+.

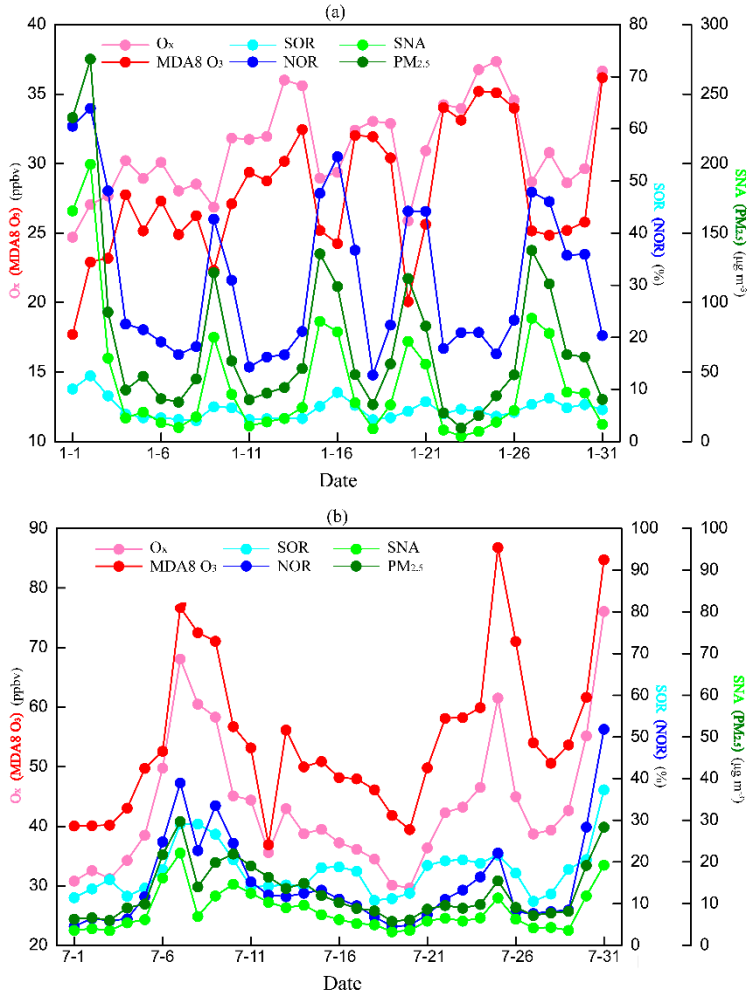

Figure 7. Time-series of simulated daily total oxidant (O_x) and MDA8 O_3 concentrations, sulfur oxidation ratio (SOR) and nitrogen oxidation ratio (NOR), as well as secondary inorganic particles (SNA) and $PM_{2.5}$ concentrations for (**a**) BTH in January and (**b**) PRD in July. The $O_x = O_3 + NO_2$, SOR = n-SO_4^{2-}/(n-SO_4^{2-} + n-SO_2), NOR = n-NO_3^-/(n-NO_3^- + n-NO_2), SNA = SO_4^{2-} + NO_3^- + NH_4^+.

For PRD in July (Figure 7b), the correlation coefficient between MDA8 O_3 and O_x was 0.93, indicating the important role of O_3 on the atmospheric oxidizing capacity. The SOR (NOR) exhibited

a pronounced positive correlation with O_x, with a high correlation coefficient of 0.89 (0.93), which indicates that the formation of secondary inorganic particulates can be promoted by photochemical oxidation and O_3. Consequently, the SNA and $PM_{2.5}$ were positively correlated with O_x and MDA8 O_3 concentrations. It is noted that high concentrations of O_3 and strong atmospheric photochemical reactions may also enhance the formation of secondary organic aerosol (SOA) [19]. By analyzing concentrations of SOA and gas pollutants measured in the summer of 2013, Wang et al. [19] found that SOA had a good correlation with O_x, with a correlation coefficient of 0.90, which indicated that SOA formation was mainly promoted by photochemical oxidation. In contrast, the correlation between SOR (NOR) and O_x was much smaller and even negative for BTH in January (Figure 7a). In general, high air temperature means strong solar radiation and high O_3 concentration. Therefore, the promoting effect of high O_3 concentration and active photochemical activity on secondary $PM_{2.5}$ formation was more effective under high temperature conditions.

Overall, in an environment of high temperature, high concentration of O_3 indicates a strong atmospheric photochemical reactivity, and significantly promotes the level of atmospheric oxidation. The strong atmospheric oxidation capacity, in turn, enhances the formation of both secondary inorganic particulates and secondary organic particulates. The enhanced formation of secondary particulates eventually leads to significant positive $PM_{2.5}$–O_3 correlation in a hot environment.

4. Conclusions and Discussion

In this study, the spatial-temporal characteristics of the correlations between $PM_{2.5}$ and O_3 were investigated at the national-scale level, based on the pollutant concentrations measured at all monitoring sites in China from the Ministry of Ecological and Environment for the whole year of 2016. The underlying reasons or mechanisms on the varying $PM_{2.5}$–O_3 correlations in different regions and seasons were examined by a chemical transport model (GEOS–Chem).

Measurements showed that the $PM_{2.5}$ concentrations were positively correlated with O_3 concentrations for most regions and seasons over China, while the negative correlations were mainly observed in northern China during winter. The strongest positive $PM_{2.5}$–O_3 correlations with correlation coefficients (r) larger than +0.7 existed in southern China during July, and the strongest negative correlations ($r < -0.5$) were observed in northern China during January.

It was very interesting to see that the spatial-temporal distributions of $PM_{2.5}$–O_3 correlations highly resembled those of temperature. Therefore, the relations between $PM_{2.5}$–O_3 correlations and temperature were further investigated. Regularly, the positive $PM_{2.5}$–O_3 correlations prevailed for high air temperature samples, while the negative correlations were generally found in a cold environment.

We then focused on comparing data points which exhibited the strongest positive $PM_{2.5}$–O_3 correlations and high air temperature (i.e., southern China in July) and those that exhibited the strongest negative $PM_{2.5}$–O_3 correlations and low air temperature (i.e., northern China in January) to investigate the underlying reasons for the varying $PM_{2.5}$–O_3 correlations for different regions and seasons (i.e., different temperature), based on the GEOS-Chem simulation. Model evaluations showed that it was viable and reliable to conduct $PM_{2.5}$–O_3 correlation analysis using the GEOS-Chem model.

The $PM_{2.5}$ may suppress O_3 generation by reducing photolysis rates. For northern China in January (i.e., low temperature condition), the average $PM_{2.5}$ concentrations were relatively high, which led to a more effective inhibitory effect of $PM_{2.5}$ on O_3 generation for cold environments than for hot environments. Therefore, the negative $PM_{2.5}$–O_3 correlation for a cold environment may be partly attributed to the effective inhibitory effect of $PM_{2.5}$ on O_3 generation by reducing photolysis rates at low temperature. The NO may suppress O_3 production through the NO titration effect, and the inhibitory effect was found to be stronger for low temperature conditions than for high temperature conditions. However, the freshly emitted NO presented a significant positive correlation with the primary particulate BC, and consequently, with $PM_{2.5}$ in cold seasons. Therefore, the negative $PM_{2.5}$–O_3 correlation at low temperature may also be partly attributed to the strong titration effect of high NO concentration, which was consistent with primary $PM_{2.5}$ in a cold environment. High concentration

of O_3 generally indicates active photochemical activity, which may promote the secondary $PM_{2.5}$ formation. In general, high O_3 concentration occurs in an environment of high temperature and strong solar radiation. Therefore, the positive $PM_{2.5}$–O_3 correlation in a hot environment may be a result of the promoting effect of high O_3 concentration and active photochemical activity on secondary particle formation.

In conclusion, the effective inhibitory effect of $PM_{2.5}$ on O_3 generation by reducing photolysis rates at low temperature, and the strong titration effect of freshly emitted NO with O_3 in cold seasons, together contribute to the strongest negative $PM_{2.5}$–O_3 correlation in cold environments. The strongest positive $PM_{2.5}$–O_3 correlation at high temperature, however, is mainly attributed to the promoting effect of high O_3 concentration and active photochemical activity on secondary particle formation in hot environments.

This paper revealed three underlying reasons for the $PM_{2.5}$–O_3 correlations. It is noted that heterogeneous chemical reaction is an important way for $PM_{2.5}$–O_3 interaction [17,59–62], which may also be a reason for the $PM_{2.5}$–O_3 correlations. The formation of SOA with high O_3 concentration may contribute to positive correlations, because biogenic emission of VOCs is high under high temperature conditions in summer [20,25]. Furthermore, the variations in meteorological variables, through affecting transport and chemical processes of pollutants, may be important for daily variations in $PM_{2.5}$ and O_3, and therefore, contribute to the $PM_{2.5}$–O_3 correlations. Comprehensively understanding all these chemical and physical mechanisms needs more in-depth research through sensitivity experiments in future studies.

Supplementary Materials: The following are available online at http://www.mdpi.com/2073-4433/10/7/352/s1, Figure S1: Spatial-temporal distributions of surface temperature (°C). Each panel represents each month for year 2016.

Author Contributions: Conceptualization, J.Z. and H.L.; Formal analysis, J.Z. and L.C.; Funding acquisition, J.Z. and H.L.; Investigation, J.Z. and R.D.; Methodology, J.Z.; Software, L.C.; Validation, R.D.; Visualization, L.C.; Writing—original draft, J.Z.; Writing—review and editing, H.L.

Funding: This research was funded by the University Natural Science Research Foundation of Jiangsu Province: 18KJB170012, the Startup Foundation for Introducing Talent of NUIST: 2018r007, the National Natural Science Foundation of China: 91744311, and the Postgraduate Research and Practice Innovation Program of Jiangsu Province: KYCX18_1018.

Acknowledgments: This study was supported by the University Natural Science Research Foundation of Jiangsu Province (18KJB170012), the Startup Foundation for Introducing Talent of NUIST (2018r007), the National Natural Science Foundation of China (91744311), and the Postgraduate Research and Practice Innovation Program of Jiangsu Province (KYCX18_1018). The authors acknowledge the free use of monitoring air quality data provided by the Ministry of Ecological and Environment (MEE) and the meteorological data of surface temperature provided by the European Centre for Medium-Range Weather Forecasts (ECMWF). We also appreciate the anonymous reviewers for their constructive comments and thoughtful suggestions.

Conflicts of Interest: The authors declare no conflict of interest.

References

1. Maji, K.J.; Dikshit, A.K.; Arora, M.; Deshpande, A. Estimating premature mortality attributable to $PM_{2.5}$ exposure and benefit of air pollution control policies in China for 2020. *Sci. Total Environ.* **2018**, *612*, 683–693. [CrossRef] [PubMed]
2. Wang, Q.; Wang, J.; He, M.Z.; Kinney, P.L.; Li, T. A county-level estimate of $PM_{2.5}$ related chronic mortality risk in china based on multi-model exposure data. *Env. Int.* **2018**, *110*, 105–112. [CrossRef] [PubMed]
3. Jeensorn, T.; Apichartwiwat, P.; Jinsart, W. PM_{10} and $PM_{2.5}$ from haze smog and visibility effect in Chiang Mai Province, Thailand. *App. Envi. Res.* **2018**, *40*, 1–10.
4. Li, Y.C.; Shu, M.; Ho, S.S.H.; Yu, J.-Z.; Yuan, Z.-B.; Wang, X.-X.; Zhao, X.-Q.; Liu, Z.-F. Effects of chemical composition of $PM_{2.5}$ on visibility in a semi-rural city of sichuan basin. *Aerosol Air Qual. Res.* **2018**, *18*, 957–968. [CrossRef]

5. Yang, C.; Yang, H.; Guo, S.; Wang, Z.; Xu, X.; Duan, X.; Kan, H. Alternative ozone metrics and daily mortality in Suzhou: The China air pollution and health effects study (CAPES). *Sci. Total Env.* **2012**, *426*, 83–89. [CrossRef] [PubMed]
6. Tai, A.P.K.; Martin, M.V.; Heald, C.L. Threat to future global food security from climate change and ozone air pollution. *Nat. Clim. Chang.* **2014**, *4*, 817–821. [CrossRef]
7. Yue, X.; Unger, N. Ozone vegetation damage effects on gross primary productivity in the United States. *Atmos. Chem. Phys.* **2014**, *14*, 9137–9153. [CrossRef]
8. Raza, A.; Dahlquist, M.; Lind, T.; Ljungman, P.L.S. Susceptibility to short-term ozone exposure and cardiovascular and respiratory mortality by previous hospitalizations. *Env. Health* **2018**, *17*, 37. [CrossRef]
9. Gao, Y.; Zhang, M. Sensitivity analysis of surface ozone to emission controls in Beijing and its neighboring area during the 2008 Olympic Games. *J. Env. Sci.* **2012**, *24*, 50–61. [CrossRef]
10. Gao, Y.; Zhang, M.; Liu, Z.; Wang, L.; Wang, P.; Xia, X.; Tao, M.; Zhu, L. Modeling the feedback between aerosol and meteorological variables in the atmospheric boundary layer during a severe fog–haze event over the North China Plain. *Atmos. Chem. Phys.* **2015**, *15*, 4279–4295. [CrossRef]
11. Wang, Y.; Zhang, Y.; Hao, J.; Luo, M. Seasonal and spatial variability of surface ozone over China: Contributions from background and domestic pollution. *Atmos. Chem. Phys.* **2011**, *11*, 3511–3525. [CrossRef]
12. Li, K.; Jacob, D.J.; Liao, H.; Shen, L.; Zhang, Q.; Bates, K.H. Anthropogenic drivers of 2013–2017 trends in summer surface ozone in China. *Proc. Natl. Acad. Sci. USA* **2019**, *116*, 422–427. [CrossRef] [PubMed]
13. Li, K.; Liao, H.; Zhu, J.; Moch, J.M. Implications of RCP emissions on future $PM_{2.5}$ air quality and direct radiative forcing over China. *J. Geophys. Res. Atmos.* **2016**, *121*, 12985–13008. [CrossRef]
14. Wang, T.; Xue, L.; Brimblecombe, P.; Lam, Y.F.; Li, L.; Zhang, L. Ozone pollution in china: A review of concentrations, meteorological influences, chemical precursors, and effects. *Sci. Total Env.* **2017**, *575*, 1582–1596. [CrossRef] [PubMed]
15. Tao, M.; Chen, L.; Wang, Z.; Wang, J.; Tao, J.; Wang, X. Did the widespread haze pollution over China increase during the last decade? A satellite view from space. *Env. Res. Lett.* **2016**, *11*, 054019. [CrossRef]
16. Tao, M.; Chen, L.; Xiong, X.; Zhang, M.; Ma, P.; Tao, J.; Wang, Z. Formation process of the widespread extreme haze pollution over northern China in January 2013: Implications for regional air quality and climate. *Atmos. Env.* **2014**, *98*, 417–425. [CrossRef]
17. Stadtler, S.; Simpson, D.; Schröder, S.; Taraborrelli, D.; Bott, A.; Schultz, M. Ozone impacts of gas–aerosol uptake in global chemistry transport models. *Atmos. Chem. Phys.* **2018**, *18*, 3147–3171. [CrossRef]
18. Pathak, R.K.; Wu, W.S.; Wang, T. Summertime $PM_{2.5}$ ionic species in four major cities of China: Nitrate formation in an ammonia-deficient atmosphere. *Atmos. Chem. Phys.* **2009**, *9*, 1711–1722. [CrossRef]
19. Wang, D.; Zhou, B.; Fu, Q.; Zhao, Q.; Zhang, Q.; Chen, J.; Yang, X.; Duan, Y.; Li, J. Intense secondary aerosol formation due to strong atmospheric photochemical reactions in summer: Observations at a rural site in eastern Yangtze River Delta of China. *Sci. Total Env.* **2016**, *571*, 1454–1466. [CrossRef]
20. Ding, A.J.; Fu, C.B.; Yang, X.Q.; Sun, J.N.; Zheng, L.F.; Xie, Y.N.; Herrmann, E.; Nie, W.; Petäjä, T.; Kerminen, V.M.; et al. Ozone and fine particle in the western Yangtze River Delta: An overview of 1 yr data at the SORPES station. *Atmos. Chem. Phys.* **2013**, *13*, 5813–5830. [CrossRef]
21. Wang, Y.; Ying, Q.; Hu, J.; Zhang, H. Spatial and temporal variations of six criteria air pollutants in 31 provincial capital cities in China during 2013–2014. *Env. Int.* **2014**, *73*, 413–422. [CrossRef]
22. Jia, M.; Zhao, T.; Cheng, X.; Gong, S.; Zhang, X.; Tang, L.; Liu, D.; Wu, X.; Wang, L.; Chen, Y. Inverse relations of $PM_{2.5}$ and O_3 in air compound pollution between cold and hot seasons over an urban area of east China. *Atmosphere* **2017**, *8*, 59. [CrossRef]
23. Tang, B.Y.; Xin, J.Y.; Gao, W.K.; Shao, P.; Su, H.J.; Wen, T.X.; Song, T.; Fan, G.Z.; Wang, S.G.; Wang, Y.S. Characteristics of complex air pollution in typical cities of North China. *Atmos. Ocean. Sci. Lett.* **2018**, *11*, 29–36. [CrossRef]
24. Zhao, H.; Zheng, Y.; Li, C. spatiotemporal distribution of $PM_{2.5}$ and O_3 and their interaction during the summer and winter seasons in Beijing, China. *Sustainability* **2018**, *10*, 4519. [CrossRef]
25. Chen, H.; Zhuang, B.; Liu, J.; Wang, T.; Li, S.; Xie, M.; Li, M.; Chen, P.; Zhao, M. Characteristics of ozone and particles in the near-surface atmosphere in the urban area of the Yangtze River Delta, China. *Atmos. Chem. Phys.* **2019**, *19*, 4153–4175. [CrossRef]

26. Tie, X.X.; Madronich, S.; Walters, S.; Edwards, D.P.; Ginoux, P.; Mahowald, N.; Zhang, R.Y.; Lou, C.; Brasseur, G. Assessment of the global impact of aerosols on tropospheric oxidants. *J. Geophys. Res.* **2005**, *110*, D03204. [CrossRef]
27. Menon, S.; Unger, N.; Koch, D.; Francis, J.; Garrett, T.; Sednev, I.; Shindell, D.; Streets, D. Aerosol climate effects and air quality impacts from 1980 to 2030. *Env. Res. Lett.* **2008**, *3*, 024004. [CrossRef]
28. Unger, N.; Menon, S.; Koch, D.M.; Shindell, D.T. Impacts of aeroso-cloud interaction on past and future changes in tropospheric composition. *Atmos. Chem. Phys.* **2009**, *9*, 4115–4130. [CrossRef]
29. Li, J.; Wang, Z.; Wang, X.; Yamaji, K.; Takigawa, M.; Kanaya, Y.; Pochanart, P.; Liu, Y.; Irie, H.; Hu, B.; et al. Impacts of aerosols on summertime tropospheric photolysis frequencies and photochemistry over Central Eastern China. *Atmos. Env.* **2011**, *45*, 1817–1829. [CrossRef]
30. Li, M.; Wang, T.; Xie, M.; Li, S.; Zhuang, B.; Chen, P.; Huang, X.; Han, Y. Agricultural fire impacts on ozone photochemistry over the Yangtze River Delta region, East China. *J. Geophys. Res.-Atmos.* **2018**, *123*, 6605–6623. [CrossRef]
31. Real, E.; Sartelet, K. Modeling of photolysis rates over Europe: Impact on chemical gaseous species and aerosols. *Atmos. Chem. Phys.* **2011**, *11*, 1711–1727. [CrossRef]
32. Khoder, M.I. Atmospheric conversion of sulfur dioxide to particulate sulfate and nitrogen dioxide to particulate nitrate and gaseous nitric acid in an urban area. *Chemosphere* **2002**, *49*, 675–684. [CrossRef]
33. Chang, S.C.; Lee, C.T. Secondary aerosol formation through photochemical reactions estimated by using air quality monitoring data in Taipei City from 1994 to 2003. *Atmos. Env.* **2007**, *41*, 4002–4017. [CrossRef]
34. Li, L.; Chen, C.H.; Huang, C.; Huang, H.Y.; Zhang, G.F.; Wang, Y.J.; Wang, H.L.; Lou, S.R.; Qiao, L.P.; Zhou, M.; et al. Process analysis of regional ozone formation over the Yangtze River Delta, China using the Community Multi-scale Air Quality modeling system. *Atmos. Chem. Phys.* **2012**, *12*, 10971–10987. [CrossRef]
35. Seinfeld, J.H.; Pandis, S.N. *Atmospheric Chemistry and Physics: From Air Pollution to Climate Change*, 3rd ed.; John Wiley & Sons, Inc.: Hoboken, NJ, USA, 2016.
36. Xu, X.; Shi, X.; Xie, L.; Ding, G.; Miao, Q.; Ma, J.; Zheng, X. Spatial characteristics of urban gaseous and particulate pollutants in winter and summer. *Sci. China Ser. D* **2005**, *35*, 53–65. [CrossRef]
37. Xiao, Z.M.; Zhang, Y.F.; Hong, S.M.; Bi, X.H.; Jiao, L.; Feng, Y.C.; Wang, Y.Q. Estimation of the main factors influencing haze, based on a long-term monitoring campaign in Hangzhou, China. *Aerosol Air Qual. Res.* **2011**, *11*, 873–882. [CrossRef]
38. Shi, C.; Wang, S.; Liu, R.; Zhou, R.; Li, D.; Wang, W.; Li, Z.; Cheng, T.; Zhou, B. A study of aerosol optical properties during ozone pollution episodes in 2013 over Shanghai, China. *Atmos. Res.* **2015**, *153*, 235–249. [CrossRef]
39. Zhang, Y.Y.; Jia, Y.; Li, M.; Hou, L.A. Spatiotemporal variations and relationship of PM and gaseous pollutants based on gray correlation analysis. *J. Env. Sci. Health A Tox. Hazard. Subst. Env. Eng.* **2018**, *53*, 139–145. [CrossRef]
40. Dee, D.P.; Uppala, S.M.; Simmons, A.J.; Berrisford, P.; Poli, P.; Kobayashi, S.; Andrae, U.; Balmaseda, M.A.; Balsamo, G.; Bauer, P.; et al. The ERA-Interim reanalysis: Configuration and performance of the data assimilation system. *Q. J. Roy. Meteor. Soc.* **2011**, *137*, 553–597. [CrossRef]
41. Wang, X.; Dickinson, R.E.; Su, L.; Zhou, C.; Wang, K. $PM_{2.5}$ pollution in China and how it has been exacerbated by terrain and meteorological conditions. *B. Am. Meteorol. Soc.* **2018**, *99*, 105–119. [CrossRef]
42. Zhong, J.; Zhang, X.; Wang, Y.; Wang, J.; Shen, X.; Zhang, H.; Wang, T.; Xie, Z.; Liu, C.; Zhang, H.; et al. The two-way feedback mechanism between unfavorable meteorological conditions and cumulative aerosol pollution in various haze regions of China. *Atmos. Chem. Phys.* **2019**, *19*, 3287–3306. [CrossRef]
43. Travis, K.R.; Jacob, D.J.; Fisher, J.A.; Kim, P.S.; Marais, E.A.; Zhu, L.; Yu, K.; Miller, C.C.; Yantosca, R.M.; Sulprizio, M.P.; et al. Why do models overestimate surface ozone in the Southeast United States? *Atmos. Chem. Phys.* **2016**, *16*, 13561–13577. [CrossRef] [PubMed]
44. Gelaro, R.; McCarty, W.; Suárez, M.J.; Todling, R.; Molod, A.; Takacs, L.; Randles, C.A.; Darmenov, A.; Bosilovich, M.G.; Reichle, R.; et al. The modern-era retrospective analysis for research and applications, version 2 (MERRA-2). *J. Clim.* **2017**, *30*, 5419–5454. [CrossRef]
45. Li, M.; Zhang, Q.; Kurokawa, J.-I.; Woo, J.-H.; He, K.; Lu, Z.; Ohara, T.; Song, Y.; Streets, D.G.; Carmichael, G.R.; et al. MIX: A mosaic Asian anthropogenic emission inventory under the international collaboration framework of the MICS-Asia and HTAP. *Atmos. Chem. Phys.* **2017**, *17*, 935–963. [CrossRef]

46. Zheng, B.; Tong, D.; Li, M.; Liu, F.; Hong, C.; Geng, G.; Li, H.; Li, X.; Peng, L.; Qi, J.; et al. Trends in China's anthropogenic emissions since 2010 as the consequence of clean air actions. *Atmos. Chem. Phys.* **2018**, *18*, 14095–14111. [CrossRef]
47. Van der Werf, G.R.; Randerson, J.T.; Giglio, L.; Collatz, G.J.; Mu, M.; Kasibhatla, P.S.; Morton, D.C.; DeFries, R.S.; Jin, Y.; van Leeuwen, T.T. Global fire emissions and the contribution of deforestation, savanna, forest, agricultural, and peat fires (1997–2009). *Atmos. Chem. Phys.* **2010**, *10*, 11707–11735. [CrossRef]
48. Mu, Q.; Liao, H. Simulation of the interannual variations of aerosols in China: Role of variations in meteorological parameters. *Atmos. Chem. Phys.* **2014**, *14*, 9597–9612. [CrossRef]
49. Yang, Y.; Liao, H.; Lou, S. Decadal trend and interannual variation of outflow of aerosols from East Asia: Roles of variations in meteorological parameters and emissions. *Atmos. Env.* **2015**, *100*, 141–153. [CrossRef]
50. Wang, Y.; Shen, L.; Wu, S.; Mickley, L.; He, J.; Hao, J. Sensitivity of surface ozone over China to 2000–2050 global changes of climate and emissions. *Atmos. Env.* **2013**, *75*, 374–382. [CrossRef]
51. Zhu, J.; Liao, H. Future ozone air quality and radiative forcing over China owing to future changes in emissions under the Representative Concentration Pathways (RCPs). *J. Geophys. Res.-Atmos.* **2016**, *121*, 1978–2001. [CrossRef]
52. Zhu, J.; Liao, H.; Mao, Y.; Yang, Y.; Jiang, H. Interannual variation, decadal trend, and future change in ozone outflow from East Asia. *Atmos. Chem. Phys.* **2017**, *17*, 3729–3747. [CrossRef]
53. Xie, M.; Zhu, K.; Wang, T.; Chen, P.; Han, Y.; Li, S.; Zhuang, B.; Shu, L. Temporal characterization and regional contribution to O_3 and NO_x at an urban and a suburban site in Nanjing, China. *Sci. Total Environ.* **2016**, *551*, 533–545. [CrossRef] [PubMed]
54. Clapp, L.J.; Jenkin, M.E. Analysis of the relationship between ambient levels of O_3, NO_2 and NO as a function of NO_x in the UK. *Atmos. Env.* **2001**, *35*, 6391–6405. [CrossRef]
55. Colbeck, I.; Harrison, R.M. Ozone—Secondary aerosol—Visibility relationships in North-West England. *Sci. Total Env.* **1984**, *34*, 87–100. [CrossRef]
56. Du, H.; Kong, L.; Cheng, T.; Chen, J.; Du, J.; Li, L.; Xia, X.; Leng, C.; Huang, G. Insights into summertime haze pollution events over Shanghai based on online water-soluble ionic composition of aerosols. *Atmos. Env.* **2011**, *45*, 5131–5137. [CrossRef]
57. Cao, Z.; Zhou, X.; Ma, Y.; Wang, L.; Wu, R.; Chen, B.; Wang, W. The concentrations, formations, relationships and modeling of sulfate, nitrate and ammonium (SNA) aerosols over China. *Aerosol Air Qual. Res.* **2017**, *17*, 84–97. [CrossRef]
58. Zhang, R.; Sun, X.; Shi, A.; Huang, Y.; Yan, J.; Nie, T.; Yan, X.; Li, X. Secondary inorganic aerosols formation during haze episodes at an urban site in Beijing, China. *Atmos. Env.* **2018**, *177*, 275–282. [CrossRef]
59. Ravishankara, A.R. Heterogeneous and multiphase chemistry in the troposphere. *Science* **1997**, *276*, 1058–1065. [CrossRef]
60. Martin, R.V.; Jacob, D.J.; Yantosca, R.M.; Chin, M.; Ginoux, P. Global and regional decreases in tropospheric oxidants from photochemical effects of aerosols. *J. Geophys. Res. Atmos.* **2003**, *108*, 4097. [CrossRef]
61. Deng, J.; Wang, T.; Liu, L.; Jiang, F. Modeling heterogeneous chemical processes on aerosol surface. *Particuology* **2010**, *8*, 308–318. [CrossRef]
62. Lou, S.; Liao, H.; Zhu, B. Impacts of aerosols on surface-layer ozone concentrations in China through heterogeneous reactions and changes in photolysis rates. *Atmos. Env.* **2014**, *85*, 123–138. [CrossRef]